Applied Surface Science 290 (2014) 368–372

Contents lists available at ScienceDirect

Applied Surface Science

journal homepage: www.elsevier.com/locate/apsusc

Ultrafast pump-probe microscopy reveals the mechanism of selective fs laser structuring of transparent thin films for maskless micropatterning

Stephan Rapp[a,*], Janosch Rosenberger[a], Matthias Domke[a], Gerhard Heise[a], Heinz P. Huber[a], Michael Schmidt[b]

[a] Munich University of Applied Sciences, Lothstrasse 34, 80335 Munich, Germany
[b] Friedrich-Alexander Universität Erlangen-Nürnberg, Lehrstuhl für Photonische Technologien, Paul Gordan Straße 3, 91052 Erlangen, Germany

ARTICLE INFO

Article history:
Received 27 June 2013
Received in revised form 23 October 2013
Accepted 17 November 2013
Available online 23 November 2013

Keywords:
Laser ablation
Pump-probe microscopy
Thin film
Ultra-short pulse laser

ABSTRACT

Maskless patterning of biocompatible Ta_2O_5/Pt/glass sensor chips can be realized by ultra-short laser pulse ablation. At a fluence of 0.2 J/cm^2, the thin Ta_2O_5 film is selectively lifted-off by indirectly-induced ablation at laser wavelenghts where the Ta_2O_5 is transparent and the Pt absorbing. This enables precise and very fast structuring. Here, 660 fs laser pulses at a center wavelength of 1053 nm are applied. The driving physical effects of this ablation mechanism are revealed by pump-probe microscopy. This technique allows the observation of the whole ablation process ranging temporally from femtoseconds to microseconds. An ultrafast heat-expansion in the absorbing Pt, initiating a shock-wave to the Ta_2O_5 within the first 10 ps, bulges the Ta_2O_5 film after some nanoseconds. Bulging velocities of 750 m/s are determined corresponding to an extreme acceleration of about 10^{10} g. Exceeding the stress limit in the Ta_2O_5 causes film disintegration after 50 ns. A model, describing essential reaction steps, is developed. This model is also applicable to other industrial important layer systems, where thin transparent films have to be removed.

1. Introduction

Thin film systems play an important role in state-of-the-art industrial technologies used for e.g., thin-film solar cells and biosensor chips. The latter are applied in life sciences for biological screening and molecular diagnostics. Advantages of these biocompatible sensor chips are their compactness and their ability to parallelize measurements [1,2]. They allow to analyze electrical properties or signals of living cells. The electrodes of the here investigated sensor chip are structured out of a conducting platinum (Pt) layer sandwiched between an isolating tantalum pentoxide (Ta_2O_5) film on top and glass substrate below (Fig. 1(a)). Laser processing enables fast and cost efficient structuring of various chip patterns in contrast to photolithography, where each design affords a new mask.

For the electrical contacting of the electrodes, the Ta_2O_5 has to be removed locally from the underlying Pt. If the chip is laser treated at a wavelength of 1053 nm, the Ta_2O_5 is transparent and the laser energy is absorbed in the Pt layer (Fig. 1(a)). The Ta_2O_5 can be lifted-off on a circular area by a single laser pulse. The resulting ablation spots – almost ideal blind holes – are free from thermal effects like cracks or burrs and the Pt shows no damages [3]. A confocal image of the described ablation spot in a 100 nm thin Ta_2O_5 layer is shown in Fig. 1(b) and the corresponding cross section in Fig. 1(c). The observed ablation type can also be found in other thin film systems, where a transparent film is removed from a massive absorbing substrate [4–8]. The needed fluence for the ablation of about 0.1 J/cm^2 is too low for an evaporation process [3]. Thus, other physical mechanisms have to be involved causing the ablation.

A simple explanation of the so called "indirectly-induced ablation" was, that the pulse energy is absorbed and maintained within an only few 10 nm thick Pt interface layer due to the short metallic absorption length and due to the also short heat dissipation length for ultra-short laser pulses [9,10]. It was suggested, that the ultrafast heating could result in an expansion, either by the solid, liquid or vapor phase of this interface layer leading to the lift-off of the overlaying Ta_2O_5 [8].

To obtain a more detailed understanding of the involved physical mechanisms, the transient behavior of the ablation process is studied in this work by imaging pump-probe microscopy. Questions that need to be addressed are: Which transient states of matter appear throughout the ablation process and when does mechanical motion begin and lead to the removal of matter?

* Corresponding author. Tel.: +49 0 8912653676.
E-mail address: rapp@hm.edu (S. Rapp).

0169-4332/$ – see front matter © 2013 Elsevier B.V. All rights reserved.
http://dx.doi.org/10.1016/j.apsusc.2013.11.086

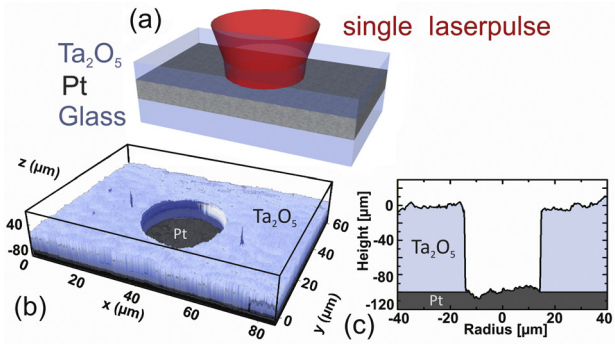

Fig. 1. Structuring method and ablated spot: (a) The laser pulse ($\lambda = 1053$ nm, $\tau = 660$ $\phi = 0.2$ J/cm^2) irradiates the sample (100 nm Ta_2O_5/200 nm Pt) and is absorbed in the Pt layer; The overlaying Ta_2O_5 is removed selectively with clean edges and without detectable thermal damages: (b) Confocal microscopy image; (c) Ablation cross section.

Pump-probe microscopy experiments with femtosecond resolution have been carried out to investigate the ablation of bulk material [11,12], the layer-side ablation of thin metal films [13,14] and the indirectly-induced ablation of SiO_2 thin films from Si [15]. The optical delay lines used were limiting maximal delay times to 10–20 ns, which is too short to monitor the actual lift-off. In contrast, nanosecond pump-probe microscopy with electronically delayed probe pulses enables infinite delay times, but does not resolve the early ultrafast steps of that process. This method was applied e.g., to study the ablation of silicone from a Ti absorber [16] and the removal from Ti or TiN layers from glass substrates [17].

To enable the observation of the entire ablation process maintaining a sub-picosecond resolution in the first 4 ns, a setup was build up combining an optically delayed probe pulse with an electronically delayed sub-nanosecond probe pulse for higher delay times [18,19]. Here, the selective removal of thin transparent Ta_2O_5 films on an absorbing Pt film and a glass substrate initiated by a 660 fs laser pulse is investigated over the whole ablation time. Therefore, ultrafast transient intensity changes of the reflected and backscattered light are analyzed.

2. Material and methods

Here the investigated layer system consists of a 200 nm thin Pt film, which is deposited by RF sputtering on a 3″ glass wafer (0.5 mm). Ta_2O_5 layers (100 and 300 nm respectively) are deposited on the Pt film by ion-assisted electron-beam evaporation.

The ablation process is analyzed by pump-probe microscopy (Fig. 2). Therefore, ultra-short laser pulses (pulse length = 660 fs FWHM; center wavelength $\lambda = 1053$ nm; repetition rate = 500 Hz) are used. A composition of a half wave plate and a polarizing beam splitter (pol. BS 1) enables the division of those pulses into pump and probe pulses (applied ratio of 90 to 10%).

On the pump-path (red), shutter 1 separates single pump pulses, which are focused on the sample (focus radius = 22 µm at e^{-2} intensity) to initiate the ablation. On the probe path, a second harmonic generation module (SHG) frequency doubles the probe pulses used for illuminating the sample on an area of about 300×300 µm^2. A linear translation stage optically delays the probe pulses up to a maximum delay time of $\Delta t = 4$ ns limited by the length of the translation stage. To enable the observation of longer delay times up to 30 µs, the initial probe path is blocked by shutter 2 and a 600 ps FWHM laser source ($\lambda = 532$ nm) emits electronically triggered probe pulses. The optical paths of the probe pulses emitted by the two different laser sources are superimposed in beam splitter 2 (pol. BS 2). A combination of a polarizing beam splitter (pol. BS 3) and a quarter wave plate allows the perpendicular illumination of the sample and its imaging by a microscope and a CCD camera (calculated optical resolution $R = 0.61$ λ/NA = 1.22 µm). To record a series of pictures at different delay times, the sample is moved to a new position for every image, irradiated by a pump pulse and illuminated by a probe pulse at the chosen delay times. Further setup information, including also the measuring procedure and the image processing, are given elsewhere [18].

The optical and electronic delay achieves a temporal resolution of 840 fs and 800 ps, respectively. These values correspond to the cross correlation times of pump and probe pulse. The ablation reaction is in both cases initiated by the 660 fs pump pulse.

The quantitative relative reflectivity change $\Delta R/R = (R_{during} - R_{before})/R_{before}$ is determined in the spot center by analyzing the grey scale value of 25 pixels (=1.4 µm^2)

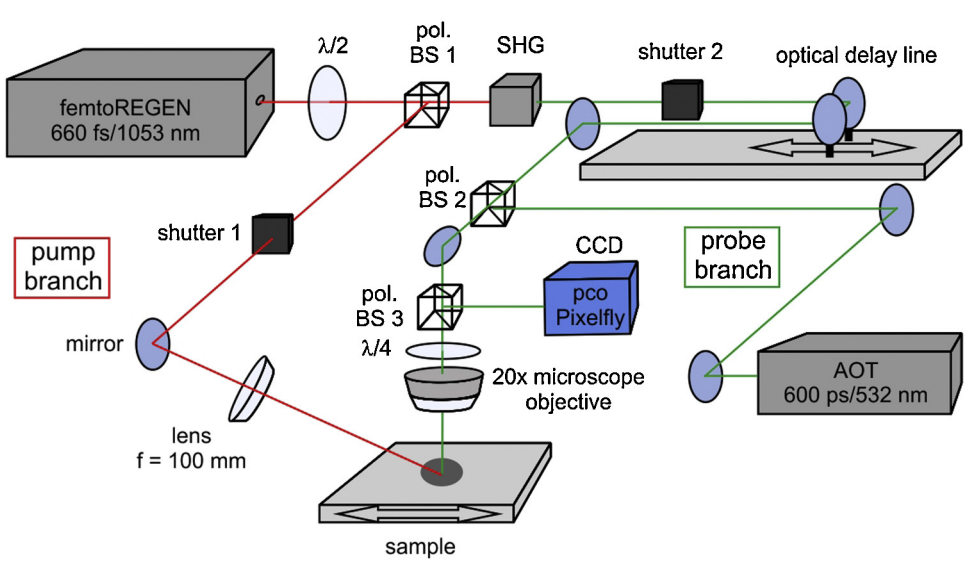

Fig. 2. Pump-probe microscopy setup: 660 fs laser pulses are divided (pol. BS 1) into pump pulses (red pump branch), initiating the reaction, and probe pulses (green probe branch), illuminating the reaction area. The probe pulses are frequency doubled (SHG) and temporally delayed by an optical delay line up to delay times of $\Delta t < 4$ ns. For $\Delta t > 4$ ns a ps laser source emits electronically triggered probe pulses. The reflected probe pulses are imaged by a microscope objective on a CCD camera.

(R_{before} = normalized reflectivity before sample irradiation; R_{during} = normalized reflectivity at Δt). Reflectivity changes >2% can be detected.

3. Results and discussion

To define appropriate structuring fluences for the selective removal of the investigated Ta_2O_5 layers, the corresponding ablation threshold fluences have to be determined. Therefore, the common method described by Liu [20] applying Eq. (1) is used.

$$D^2 = 2\omega_0^2 \ln \frac{\phi}{\phi_{thr}} \quad (1)$$

D indicates the ablated spot diameter, ω_0 the beam focus radius, ϕ_{thr} the threshold fluence, and ϕ the applied pulse peak fluence. This model, originally describing bulk material, was proven to be valid also for thin dielectric films [21] and for thin film photovoltaic materials [22]. According to Eq. (1), the experimental measured squared ablation diameters should lay on a straight line when plotted over the logarithm of the applied fluence. The intersection point of this fitted graph with the abscissa at $D^2 = 0\,cm^2$ indicates the threshold fluence ϕ_{thr}. Results show a good agreement of fitted graph and data points over more than one order of magnitude in fluence (Fig. 3). This indicates an almost ideal threshold behavior for both samples in this fluence interval. The ablation threshold fluences are determined to be $\phi_{thr} = 0.02\,J/cm^2$ (100 nm Ta_2O_5) and $\phi_{thr} = 0.07\,J/cm^2$ (300 nm Ta_2O_5) (accuracy = ±5%).

Pump-probe images of the ablation process in top view are shown in Fig. 4. Two samples with different Ta_2O_5 layer thicknesses (100 nm in the upper two rows and 300 nm in the lower two rows) are compared. The Pt layer thickness (200 nm) and the irradiation fluence just above the threshold (0.2 J/cm²) are kept constant. The corresponding delay times are indicated in the left upper corners of the recorded pictures.

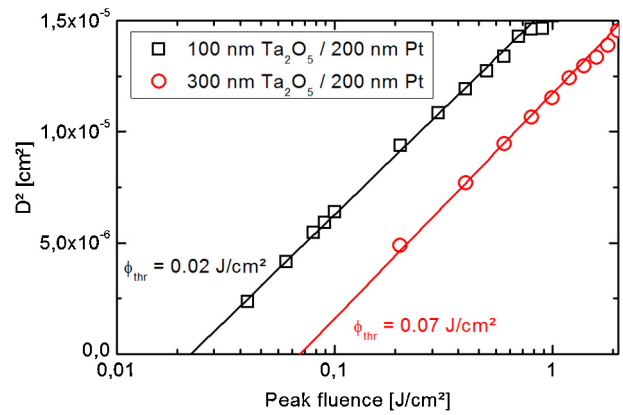

Fig. 3. Single pulse ablation threshold fluence ϕ_{thr} determination of transparent 100 nm ($\phi_{thr} = 0.02\,J/cm^2$) and 300 nm ($\phi_{thr} = 0.07\,J/cm^2$) Ta_2O_5 films on an absorbing 200 nm Pt layer. The squared ablation diameters are plotted over the applied fluence.

Around delay time zero ($\Delta t = 0$ ps) the pump pulse is transmitted through the Ta_2O_5 and absorbed by free electrons in a thin Pt interface (optical penetration depth = 14 nm; thermal penetration depth = 8 nm) [9,10].

Within the first 10 ps, a dark circle appears in the irradiated area for both layer thicknesses (Fig. 4). The relative reflectivity decreases to −30% (100 nm Ta_2O_5) and to −40% (300 nm Ta_2O_5) (Fig. 5), respectively. The free electrons in the Pt transfer their energy to the lattice leading to ultrafast heating and melting [23,24] resulting probably in a confined phase explosion [19]. At that delay time the Pt has still the density of a solid, but the mean thermal energy of a liquid or a gas. The state of matter can be described now as super-critical. The reflectivity decrease can be explained with the formation of an inhomogeneous gas-liquid mixture, scattering the probe light [11]. Similar observations were made for direct laser

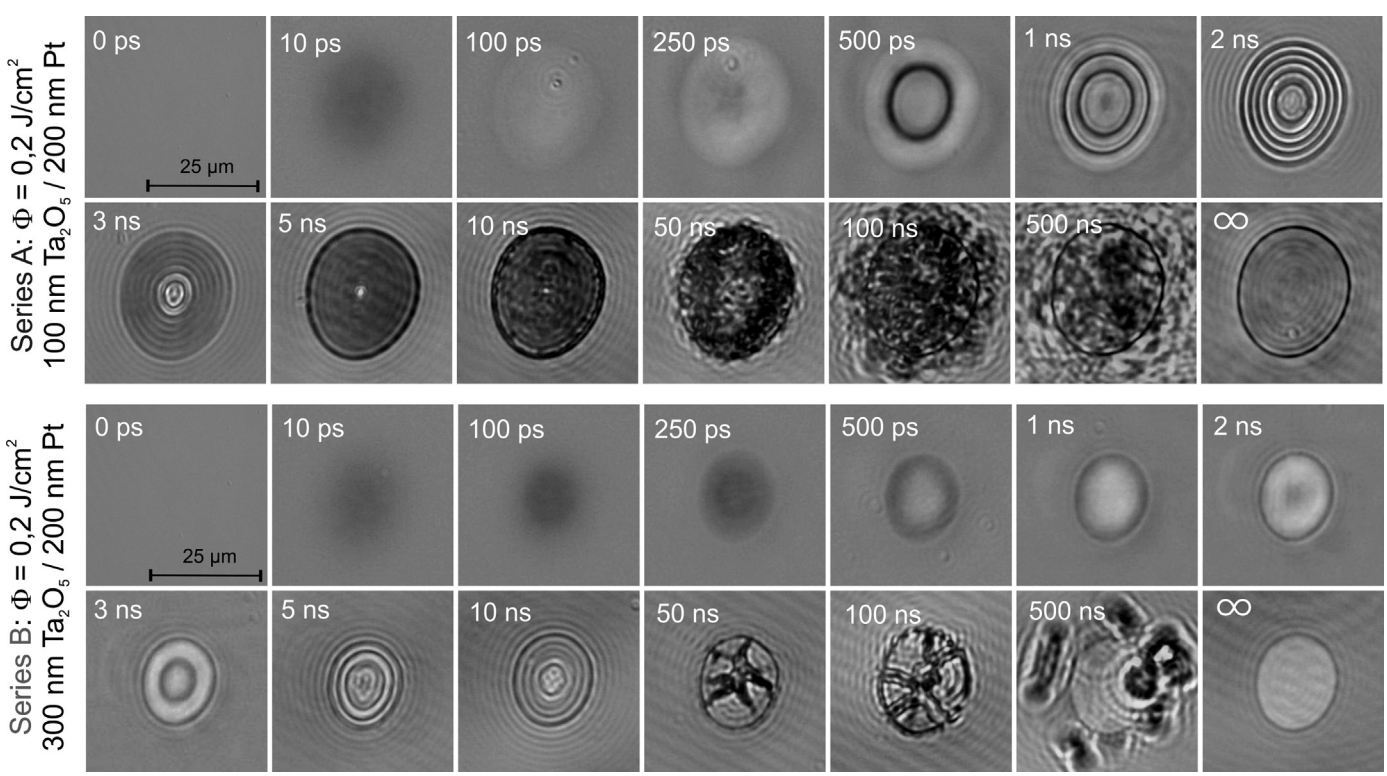

Fig. 4. Top view pump-probe images at different significant delay times (left upper corner of every image) of 100 nm (top two rows) and 300 nm (lower two rows) Ta_2O_5 on 200 nm Pt ablated with a 1053 nm/660 fs (FWHM) pulse at a pulse peak fluence of $\phi = 0.2\,J/cm^2$.

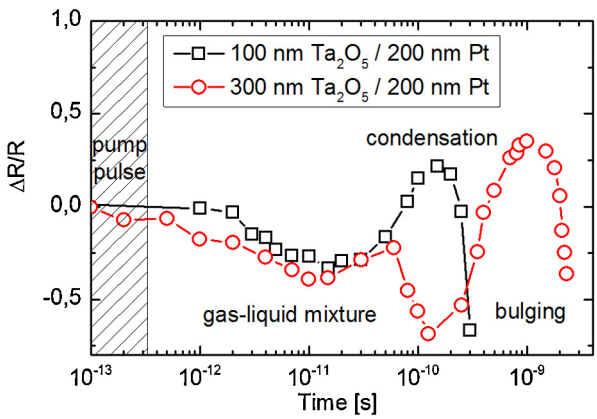

Fig. 5. Temporal change of relative reflectivity change ($\Delta R/R$) in the spot center after irradiation with a single 660 fs laser pulse at a fluence of $\phi = 0.2\,J/cm^2$. Two different layer thicknesses are investigated (black squares: 100 nm Ta_2O_5 on 200 nm Pt; red circles: 300 nm Ta_2O_5 on 200 nm Pt). (For interpretation of the references to colour in this figure legend, the reader is referred to the web version of this article.)

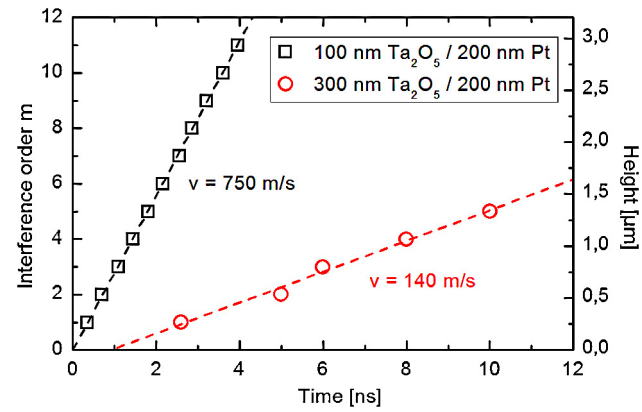

Fig. 6. Determination of the temporal layer bulging height (right axis) of two different layer thicknesses (black squares: 100 nm Ta_2O_5 on 200 nm Pt; red circles: 300 nm Ta_2O_5 on 200 nm Pt). The bulging height is calculated by analyzing the interference order of Newton's rings (left axis) by formula 1. (For interpretation of the references to colour in this figure legend, the reader is referred to the web version of this article.)

ablation of bulk metals [19] and semiconductors [11], where the material ejection of Pt would begin at this point in time. For delay times longer than 10 ps the confined ablation process differs drastically from the direct laser ablation. The inertial confinement by the transparent Ta_2O_5 is preventing the absorbing metal from evaporating out of the gas-liquid mixture. Thus, a steep rise of pressure must occur creating a shock-wave and transferring the energy from the interface layer to the transparent film [25].

After 100 ps, the irradiated spot on the sample with 100 nm Ta_2O_5 layer displays a reflectivity increase to a maximum of +25% at 200 ps (Fig. 4, upper row, and Fig. 5, black squares). The transferred energy causes the transparent layer to bulge. Adiabatic cooling due to expansion of the volume around the interface leads to condensation of the gas-liquid mixture. Thus, the observed reflectivity increase can be explained by the creation of the liquid phase and its higher reflectivity compared to the reflectivity of the solid phase.

In contrast, on the 300 nm Ta_2O_5 sample the increase of reflectivity starts delayed and has its maximum at 1 ns at a value of +35% (Fig. 4, middle row, and Fig. 5, red circles). The three times thicker Ta_2O_5 layer displays more inertia and stiffness leading to a slower mechanical reaction resulting in a delayed condensation.

The motion of the Ta_2O_5 film leads to the creation of Newton's rings – interference rings of light reflected from the curved film and the flat Pt surfaces [15]. At about 300 ps, the first Newton's ring is created on the sample with 100 nm Ta_2O_5, indicated by a second minimum in reflectivity (Fig. 5, black squares, last data point). The pump-probe image after 500 ps shows this first Newton's ring at a slightly longer delay time (Fig. 4, first row). From that delay time on the bulging height d of the Ta_2O_5 can be measured by counting these rings and applying Eq. (2)

$$d = m\frac{\lambda}{2}, \tag{2}$$

where m describes the interference order and λ the illuminating wavelength. The number of Newton's rings increases with time up to 2 ns indicating the bulging of the Ta_2O_5 dome. At 5 ns and 10 ns the number of Newton's rings is too large to be spatially resolved by the used setup (Fig. 4, upper series). On the 300 nm Ta_2O_5 sample, the creation of Newton's rings starts later at about 2 ns, when the reflectivity reaches a minimum (Figs. 4 and 5, red circles, last data point). The delayed onset confirms the argumentation of a higher layer inertia given before. The number of rings and the corresponding bulging height increase at delay times of 5 and 10 ns (Fig. 4, last row). The obtained data for both layer thicknesses are plotted in Fig. 6. A linear increase of the bulging height can be observed with constant bulging velocities of $v = 750$ m/s (100 nm Ta_2O_5) and $v = 140$ m/s (300 nm Ta_2O_5). The acceleration must have occurred at the onset of mechanical motion, that was determined to delay times of about 0.2 ns (100 nm Ta_2O_5) and 1 ns (300 nm Ta_2O_5) (Figs. 4 and 5), when delamination started. These results agree well with the height measurements in Fig. 6, when the bulging height equals zero (linearly fitted and extrapolated dotted lines), whereas, a steep acceleration has to be assumed for the 100 nm layer after 200 ps. A simple estimation shows that the acceleration value within delay times of about 1 ns has been in the order of 10^{10} to 10^{11} g.

At 50 ns the pictures of both samples show the disintegration or fracturing of the layer, when the tensile stress in the film exceeds the stress limit. Small particles – that cannot be individually resolved by the used objective – are created for the thinner

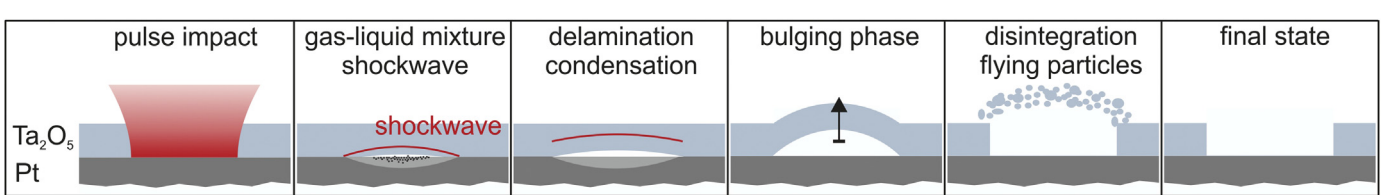

Δt (Series A): 0 s	10 ps	100 ps -250 ps	500 ps -10 ns	50 ns - 500 ns	∞
Δt (Series B): 0 s	10 ps -250 ps	500 ps -1 ns	2 ns -10 ns	50 ns - 500 ns	∞

Fig. 7. Simplified model in side view to the series of measurements (series A: 100 nm Ta_2O_5 on 200 nm Pt; series B: 300 nm Ta_2O_5 on 200 nm Pt) displayed in Fig. 4. Essential reaction steps with corresponding reaction times in the bottom two rows are shown.

layer and larger pieces for the thicker one. At 100 ns the material is leaving the depth of focus and is further propagating at 500 ns. The final state displays a clean cylindrical ablated area without detectable thermal damages in the remaining material for both layer thicknesses (Fig. 4 last pictures of both series of measurement and Fig. 1).

The observations and the state-of-the-art knowledge of surface laser ablation can be composed to the model displayed in Fig. 7. The reaction initiation – the pulse absorption in the Pt (0 ps) – is followed by energy transfer to the Pt lattice, subsequent ultrafast melting and the creation of a gas-liquid-mixture at the surface of the layer. The inertial confinement by the transparent Ta_2O_5 leads to a steep rise of pressure and temperature; both creating a shock-wave (10 ps) and an energy transfer from the interface layer to the transparent film. At around 100 ps the transparent film delaminates and the evaporated material of the absorbing layer condenses. At around 1 ns the film starts to bulge and at about 10 ns the maximum height is reached. Then, the Ta_2O_5 layer ruptures (50 ns). An almost ideal blind hole without damages is created in the remaining transparent film on the absorbing underlying layer in the final state.

4. Conclusion

In this work the temporal behavior of the selective laser ablation reaction of a transparent Ta_2O_5 film covering an absorbing Pt layer on a glass substrate has been investigated over the complete temporal process range. The generalized results are summarized in the model displayed in Fig. 7.

In summary, an ultrafast melting or evaporation in a few tens of nm thick interface layer is inducing the removal of a few hundreds of nm thick covering transparent layer. This indirectly-induced ablation mechanism allows extremely efficient laser structuring of thin transparent films.

For the described processes, a specific ablation energy [26] of 15–20 J/mm^3 can be determined. This value can be expressed in an ablation rate (removed volume per minute per Watt of applied laser power) of 3–4 mm^3 min^{-1} W^{-1}. Assuming a structuring width of 20 μm and a film thickness of 100–300 nm such an ablation rate is resulting in process speeds of about 7–10 m/s, respectively, for 1 W of irradiated laser power and an overlap of 50% (two pulses per position on average).

The described ablation principle of the indirectly-induced laser ablation can be generalized for other industrial important thin film layer systems, where transparent films are covering absorbing substrates or underlying layers. An example for such a layer system is a transparent SiO_2 or SiN_x film on a Si surface in Si solar cell manufacturing [4–6]. Another example is the structuring of the transparent ZnO front contact of a CIS thin film solar cell [7,8].

In all cases the fundamental aspect seems to be the creation of a shock-wave by ultrafast heating a few tens of nm thick interface layer on an ultrafast time scale which transfers the energy to the few hundred nm thick transparent layer. The model of the "indirectly-induced" laser ablation can be applied to all of these observations for explaining the underlying mechanisms.

Hence, by utilizing indirectly-induced laser ablation, ultrafast lasers can provide precise and selective processes at extremely high efficiencies for maskless structuring and production of thin film system devices such as solar cells and bio sensor chips.

Acknowledgement

This work was partly funded by the German Federal Ministry of Education and Research within the project "METASOLAR" under the grant No. 02PO2851.

References

[1] G.W. Gross, E. Rieske, G.W. Kreutzberg, A. Meyer, A new fixed-array multi-microelectrode system designed for long-term monitoring of extracellular single unit neuronal activity in vitro, Neurosci. Lett. 6 (2–3) (1977) 101–105.
[2] A.F.M. Johnstone, G.W. Gross, D.G. Weiss, O.H.U. Schroeder, A. Gramowski, T.J. Shafer, Microelectrode arrays: a physiologically based neurotoxicity testing platform for the 21st century, NeuroToxicol. 31 (4) (2010) 331–350.
[3] G. Heise, D. Trappendreher, F. Ilchmann, R. Weiss, B. Wolf, H. Huber, Picosecond laser structuring of thin film platinum layers covered with tantalum pentoxide isolation, J. Appl. Phys. 112 (2012) 013110.
[4] S. Hermann, N.-P. Harder, R. Brendel, D. Herzog, H. Haferkamp, Picosecond laser ablation of SiO_2 layers on silicon substrates, Appl. Phys. A 99 (1) (2010) 151–158.
[5] A.W. Blakers, A. Wang, A.M. Milne, J. Zhao, M.A. Green, 22.8% efficient silicon solar cell, Appl. Phys. Lett. 55 (13) (1989) 1363–1365.
[6] V.V. Rana, Z. Zhang, Selective removal of dielectric layers using picosecond UV pulses, Proc. SPIE 7193 (2009).
[7] G. Heise, A. Heiss, C. Hellwig, T. Kuznicki, H. Vogt, J. Palm, H.P. Huber, Optimization of picosecond laser structuring for the monolithic serial interconnetion of CIS solar cells, Prog. Photovoltaics (2012), 10.1002/pip.1261.
[8] G. Heise, M. Dickmann, M. Domke, A. Heiss, T. Kuznicki, J. Palm, I. Richter, H. Vogt, H.P. Huber, Investigation of the ablation of zinc oxide thin films on copper-indium-selenide layers by ps laser pulses, Appl. Phys. A 104 (1) (2011) 387–393.
[9] R. Iffländer, Solid-State Lasers for Materials Processing, Springer, Berlin, 2001.
[10] E.D. Palik, Handbook of Optical Constants of Solids, Academic Press, Boston, 1985.
[11] D. Von Der Linde, K. Sokolowski-Tinten, Physical mechanisms of short-pulse laser ablation, Appl. Surf. Sci. 154–155 (2000) 1–10.
[12] J. Bonse, G. Bachelier, J. Siegel, J. Solis, H. Sturm, Time- and space-resolved dynamics of ablation and optical breakdown induced by femtosecond laser pulses in indium phosphide, J. Appl. Phys. 103 (5) (2008) 054910.
[13] I. Mingareev, A. Horn, Melt dynamics of aluminum irradiated with ultrafast laser radiation at large intensities, J. Appl. Phys. 106 (1) (2009) 013513.
[14] D. Von Der Linde, K. Sokolowski-Tinten, J. Bialkowski, Laser-solid interaction in the femtosecond time regime, Appl. Surf. Sci. 109–110 (1997) 1–10.
[15] J.P. McDonald, J.A. Nees, S.M. Yalisove, Pump-probe imaging of femtosecond pulsed laser ablation of silicon with thermally grown oxide films, J. Appl. Phys. 102 (6) (2007) 063109.
[16] D.D. Dlott, Ultra-low threshold laser ablation investigated by time-resolved microscopy, Appl. Surf. Sci. 197–198 (2002) 3–10.
[17] S.G. Koulikov, D.D. Dlott, Ultrafast microscopy of laser ablation of refractory materials: ultra low threshold stress-induced ablation, J. Photochem. 145 (3) (2001) 183–194.
[18] M. Domke, S. Rapp, M. Schmidt, H.P. Huber, Ultrafast pump-probe microscopy with high temporal dynamic range, Opt. Express 20 (9) (2012) 10330–10338.
[19] M. Domke, S. Rapp, M. Schmidt, H.P. Huber, Ultra-fast movies of thin-film laser ablation, Appl. Phys. A 109 (2) (2012) 409–420.
[20] J.M. Liu, Simple technique for measurements of pulsed Gaussian-beam spot sizes, Opt. Lett. 7 (5) (1982) 196–198.
[21] J. Bonse, S. Baudach, W. Kautek, E. Welsch, J. Krüger, Femtosecond laser damage of a high reflecting mirror, Thin Solid Films 408 (1–2) (2002) 297–301.
[22] J. Bovatsek, A. Tamhankar, R.S. Patel, N.M. Bulgakova, J. Bonse, Thin film removal mechanisms in ns-laser processing of photovoltaic materials, Thin Solid Films 518 (10) (2010) 2897–2904.
[23] B. Rethfeld, K. Sokolowski-Tinten, D. Von Der Linde, S.I. Anisimov, Timescales in the response of materials to femtosecond laser excitation, Appl. Phys. A 79 (4–6) (2004) 767–769.
[24] S.K. Sundaram, E. Mazur, Inducing and probing non-thermal transitions in semiconductors using femtosecond laser pulses, Nat. Mater. 1 (4) (2002) 217–224.
[25] P. Peyre, R. Fabbro, Laser shock processing: a review of the physics and applications, Opt. Quant. Electron. 27 (12) (1995) 1213–1229.
[26] G. Heise, M. Englmaier, C. Hellwig, T. Kuznicki, S. Sarrach, H.P. Huber, Laser ablation of thin molybdenum films on transparent substrates at low fluences, Appl. Phys. A 102 (1) (2011) 173–178.